

Accepted Manuscript

Design, synthesis and biological evaluation of 1,4-Diazobicyclo[3.2.2]nonane derivatives as $\alpha 7$ -Nicotinic acetylcholine receptor PET/CT imaging agents and agonists for Alzheimer's disease

Shuxia Wang, Yu Fan, Huan Wang, Hang Gao, Guohua Jiang, Jianping Liu, Qianqian Xue, Yueheng Qi, Mengying Cao, Bingchao Qiang, Huabei Zhang

PII: S0223-5234(18)30842-0

DOI: [10.1016/j.ejmech.2018.09.064](https://doi.org/10.1016/j.ejmech.2018.09.064)

Reference: EJMECH 10775

To appear in: *European Journal of Medicinal Chemistry*

Received Date: 13 March 2018

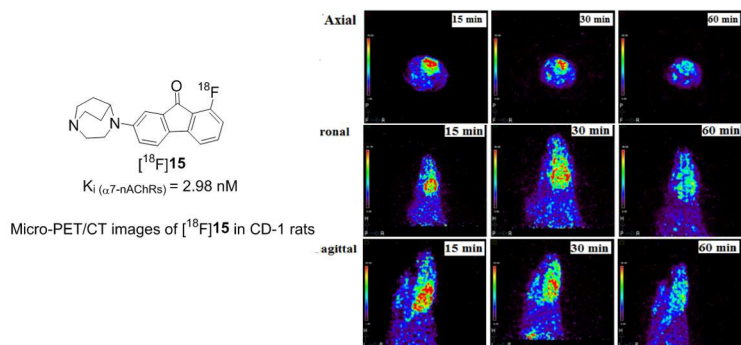
Revised Date: 20 September 2018

Accepted Date: 25 September 2018

Please cite this article as: S. Wang, Y. Fan, H. Wang, H. Gao, G. Jiang, J. Liu, Q. Xue, Y. Qi, M. Cao, B. Qiang, H. Zhang, Design, synthesis and biological evaluation of 1,4-Diazobicyclo[3.2.2]nonane derivatives as $\alpha 7$ -Nicotinic acetylcholine receptor PET/CT imaging agents and agonists for Alzheimer's disease, *European Journal of Medicinal Chemistry* (2018), doi: <https://doi.org/10.1016/j.ejmech.2018.09.064>.

This is a PDF file of an unedited manuscript that has been accepted for publication. As a service to our customers we are providing this early version of the manuscript. The manuscript will undergo copyediting, typesetting, and review of the resulting proof before it is published in its final form. Please note that during the production process errors may be discovered which could affect the content, and all legal disclaimers that apply to the journal pertain.







Design, Synthesis and Biological Evaluation of 1,4-Diazobicyclo[3.2.2]nonane Derivatives as $\alpha 7$ -Nicotinic Acetylcholine Receptor PET/CT Imaging Agents and Agonists for Alzheimer's Disease

Shuxia Wang[†], Yu Fang[†], Huan Wang, Hang Gao, Guohua Jiang, Jianping Liu, Qianqian Xue, Yueheng Qi, Mengying Cao, Bingchao Qiang, Huabei Zhang*

Key Laboratory of Radiopharmaceuticals of Ministry of Education, College of Chemistry, Beijing Normal University, Beijing 100875, China

ARTICLE INFO

Article history:

Received
Received in revised form
Accepted
Available online

Keywords:

Alzheimer's Disease (AD)
 $\alpha 7$ -Nicotinic acetylcholine receptor ($\alpha 7$ -nAChR)
1,4-Diazobicyclo[3.2.2]nonane
Radiotracer
PET/CT imaging

ABSTRACT

$\alpha 7$ -Nicotinic acetylcholine receptor ($\alpha 7$ -nAChR) agonists are promising therapeutic drug candidates for treating the cognitive impairment associated with Alzheimer's disease (AD). Thus, a novel class of derivatives of 1,4-diazobicyclo[3.2.2]nonane has been synthesized and evaluated as $\alpha 7$ -nAChR ligands. Five of them displayed high binding affinity ($K_i = 0.001$ -25 nM). In particular, the K_i of **14** was 0.0069 nM, which is superior to that of the most potent ligand that was previously reported by an order of magnitude. Four of them had high selectivity for $\alpha 7$ -nAChRs over $\alpha 4\beta 2$ -nAChRs and no significant hERG (human ether-a-go-go-related gene) inhibition. Their agonist activity was also discussed preliminarily. One of the compounds, **15** ($K_i = 2.98 \pm 1.41$ nM), was further radiolabeled with ^{18}F to afford [^{18}F]**15** for PET imaging, which exhibited high initial brain uptake ($11.60 \pm 0.14\%$ ID/g at 15 min post injection), brain/blood value (9.57 at 30 min post injection), specific labeling of $\alpha 7$ -nAChRs and fast clearance from the brain. Blocking studies demonstrated that [^{18}F]**15** was $\alpha 7$ -nAChR selective. In addition, micro-PET/CT imaging in normal rats further indicated that [^{18}F]**15** had obvious accumulation in the brain. Therefore, [^{18}F]**15** was proved to be a potential PET radiotracer for $\alpha 7$ -nAChR imaging.

©2018 Elsevier Masson SAS. All rights reserved.

1. Introduction

Alzheimer's disease (AD), the most common form of dementia, is widespread in people over 65 [1]. AD is an irreversible and progressive neurodegenerative disease characterized by memory impairment, cognitive dysfunction, language deterioration, etc. [2] AD also imposes a huge economic burden and induces psychological pressure that is predicted to be unbearable. However, the medicines currently available can provide only modest and temporary improvement in cognitive performance and are ineffective in curing AD.

Nicotinic acetylcholine receptors (nAChRs), a superfamily of ligand-gated ion channels widely expressed in the central and peripheral nervous systems [3], are pentameric structures composed of α (i.e., $\alpha 2$ - $\alpha 10$) and β (i.e., $\beta 2$ - $\beta 4$) subunits that assemble into various combinations as homopentamers or heteropentamers [4] in response to the binding of the neurotransmitter acetylcholine (ACh). Among the many subtypes in the human brain, heteromeric $\alpha 4\beta 2$ -nAChRs and homomeric $\alpha 7$ -nAChRs are the most abundant [5]. $\alpha 7$ -nAChRs are composed of five identical $\alpha 7$ subunits and mainly exist in the hippocampus, cerebral cortex and other regions associated with learning, memory and cognition [6]. $\alpha 7$ -nAChRs are also characterized by high permeability to Ca^{2+} and affinity for the

antagonists α -bungarotoxin and methyllycaconitine (MLA) [7, 8].

There is powerful evidence that $\alpha 7$ -nAChRs play a critical role in the pathogenesis of AD [9]. Many pharmacological and genetic studies and clinical trials have shown the involvement of $\alpha 7$ -nAChRs in cognitive deficits. In human studies, reduction in $\alpha 7$ -nAChR binding sites and protein levels is observed in the brains of patients with AD [10, 11]. Based on this research, there is a strong possibility that $\alpha 7$ -nAChR agonists are a potential avenue to effectively improve cognitive function in patients with AD [12].

For these reasons, $\alpha 7$ -nAChRs as a significant drug target to treat AD have received increasing interest in the fields of science and medicine. Thus, great progress in quantity and quality of $\alpha 7$ -nAChR ligands has been made over the past decades (for reviews [2, 13, 14]), including GTS-21 [15], AR-R17779 [16], SSR180711 [17], TC-5619 [18], BMS-902483 [19] (figure 1). Although some of the ligands with better properties have been proved to improve cognitive performance in animal models and clinical trials, none have been put on the market because of their limitation in structural diversity, affinity, selectivity or other side effects.

Imaging and quantifying $\alpha 7$ -nAChRs with positron-emission tomography (PET) and single-photon emission computed tomography (SPECT) might offer a non-invasive way to

□ Corresponding author.

E-mail address: hbzhang@bnu.edu.cn (Huabei Zhang)

critically facilitate the early diagnosis of $\alpha 7$ -nAChR-related CNS disorders and provide an insight into its role in AD and schizophrenia. Many leading compounds have been labeled with ^{125}I , ^{11}C or ^{18}F [20, 21], such as [^{125}I]1 [22], [^{11}C]CHIBA-1001 [23], [^{18}F]NS10743 [24], and [^{18}F]ASEM [25] (figure 1), but most of them displayed low brain uptake or specific binding. The most recent $\alpha 7$ -nAChR tracer, [^{18}F]ASEM with high specific affinity for $\alpha 7$ -nAChR ($K_i = 0.4$ nM), which was developed by Gao et al. [25], has been carried out in human studies [26, 27], and homologous [^{18}F]DBT10 [27] ($K_i = 1.3$ nM) shows similar characteristic. These two compounds are the most promising agents for human $\alpha 7$ -nAChR PET imaging.

1,4-Diazabicyclo[3.2.2]nonane as a good skeleton are widely found in $\alpha 7$ -nAChR ligands [28, 29]. And on the basis of our previous work [30, 31], herein, we report the design and synthesis of a new derivatives of 1,4-diazabicyclo[3.2.2]nonane and their evaluation as $\alpha 7$ -nAChR ligands based on their affinity, agonist activity, hERG toxicity and selectivity. Moreover, radiochemical techniques were used to label one of these compounds, **15** [32], with [^{18}F] to afford [^{18}F]15 which was biologically evaluated in mice for PET imaging of $\alpha 7$ -nAChRs.

2. Results and Discussion

2.1. Chemistry

The synthesis of the meta-substitution compounds **5**, **6** is outlined in scheme 1. Bromination and nitration of the starting material 9H-fluoren-9-one (**1**) provided 2-bromo-7-nitro-9H-fluoren-9-one (**3**), which was sequentially reacted with 1,4-diazabicyclo[3.2.2]nonane via the Buchwald-Hartwig cross-coupling reaction to afford 2-(1,4-diaza-bicyclo[3.2.2]nonan-4-yl)-7-nitro-9H-fluoren-9-one (**4**). Then, reduction of the nitro group in **4** with iron powder yielded the corresponding aniline **5**. **6** was obtained via the Schiemann reaction.

The synthesis of the ortho-substitution compounds is outlined in scheme 2. Fluoranthene (**7**) was oxidized by chromium (VI) oxide and brominated to 7-bromo-9-oxo-9H-fluorene-1-carboxylic acid (**9**) in high yields. The carboxy group in **9** was converted to a Boc-protected aniline using the Curtius rearrangement followed by tert-butyl ester formation in one pot to afford tert-butyl 2-bromo-9-oxo-9H-fluoren-8-ylcarbamate (**10**). In addition, **10** was treated with 1 M HCl to remove the N-Boc-protecting group and oxidized with 30% H_2O_2 providing 7-bromo-1-nitro-9H-fluoren-9-one (**12**). The desired compounds **14** and **15** were ultimately prepared using similar steps as **5** and **6**.

The synthesis of compounds **24**, **25** is outlined in scheme 3. The compound **21** was obtained through the methods previously reported [28].

2.2. In vitro binding assay and agonistic effects

To determine the affinity of the synthesized compounds for $\alpha 7$ -nAChRs, in vitro competition binding assays were performed with extracted rat cerebral cortex as the receptor protein and [^{125}I] α -bungarotoxin (0.4 nM), an $\alpha 7$ -nAChR antagonist ($K_D = 0.7$ nM), as the competing radioligand. Furthermore, **MLA**, an $\alpha 7$ -nAChR-selective antagonist, was also tested for confirming the reliability of the method (table 1) and for comparison. Five compounds exhibited remarkable binding affinities for $\alpha 7$ -nAChRs ($K_i = 0.001$ -25 nM). The two amino derivatives, **5** and **14**, showed two and three orders of magnitude better affinities than the reference ligand **MLA**, respectively. In particular, **14** ($K_i = 0.0069 \pm 0.004$ nM) still displayed exceptional binding to the target: its affinity was superior to that of the most potent ligand by an order of magnitude, as indicated by a rough comparison with the highest affinity compound ($K_i = 0.023$ nM [29], 0.3 nM [25]),

although the test conditions were not exactly the same. The affinities of the two fluoro ligands, **6** and **15**, were also high and were comparable to that of **MLA**. Fluoro derivative **24** also showed moderate binding affinity whereas the affinity of isomer **25** was much lower.

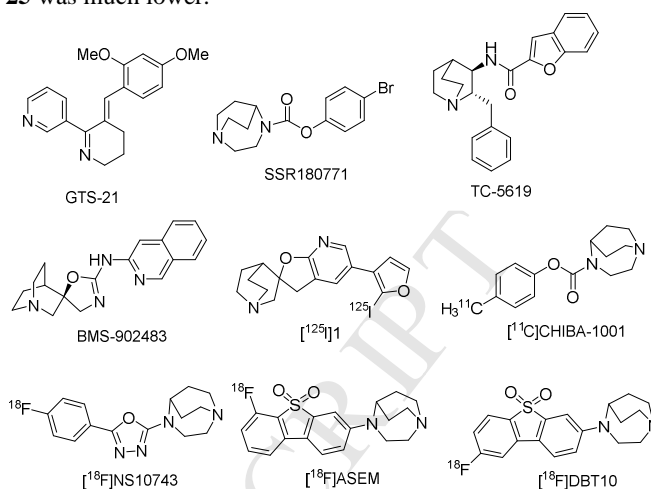


Figure 1. Representative $\alpha 7$ -nAChRs ligands and radioligands.

Heteromeric $\alpha 4\beta 2$ -nAChRs is the main cerebral subtype, so the binding assay for $\alpha 4\beta 2$ -nAChRs was also performed using [^3H]cytisine (1nM) as the competing radioligand (table 1). **5** and **14** showed high selectivity because of strong affinity for $\alpha 7$ -nAChRs. The fluoro derivatives **6** and **15** were also displayed good $\alpha 7$ -/ $\alpha 4\beta 2$ -nAChRs selectivity. Because of the excellent affinity and selectivity of these four ligands, their agonistic activities were preliminarily elucidated by a patch clamp electrophysiology assay. The result showed that none of them were strong agonists to acetylcholine ligand-gated channels at 1 μM relative to acetylcholine at 30 μM (the data analysis is shown in the supporting information).

Table 1 Binding affinities (K_i , nM) of MLA, nicotine and the 1,4-diazabicyclo[3.2.2]nonane derivatives for $\alpha 7$ -nAChRs and $\alpha 4\beta 2$ -nAChRs

Comp.	K_i (nM)		Selectivity $\alpha 7/\alpha 4\beta 2$
	$\alpha 7^a$	$\alpha 4\beta 2^b$	
MLA	2.88 \pm 0.78	nt ^c	
Nicotine	nt ^c	4.1 \pm 1.13	
5	0.064 \pm 0.058	4652 \pm 798	>10000
6	7.24 \pm 1.02	4734 \pm 653	654
14	0.0069 \pm 0.004	6656 \pm 812	>10000
15	2.98 \pm 1.41	3693 \pm 325	1239
24	21.76 \pm 1.22	nt ^c	
25	377.94 \pm 118.534	nt ^c	

^a SD rat (female) cerebral cortex; radiotracer, [^{125}I] α -bungarotoxin (0.4 nM), $K_D = 0.7$ nM; K_i values are the means \pm SD of three experiments performed in triplicate.

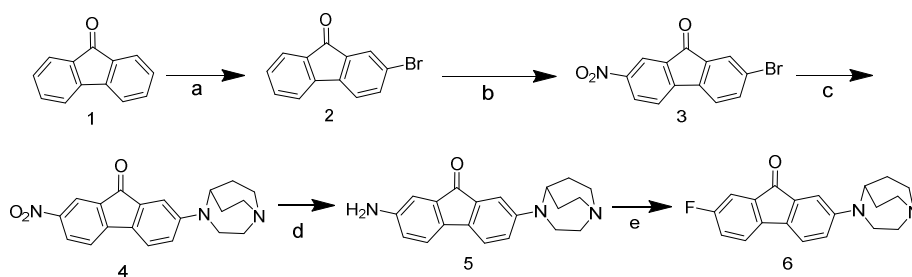
^b SD rat (female) cerebral cortex; radiotracer, [^3H]Cytisine (1 nM), $K_D = 0.77$ nM; K_i values are the means \pm SD of three experiments performed in triplicate.

^c nt: not determined.

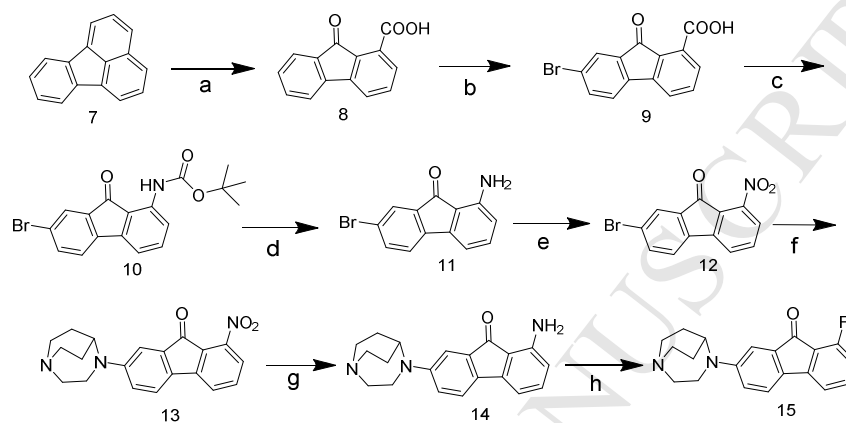
2.3. hERG assay

Inhibition of the hERG potassium channels may introduce QT interval prolongation, thereby causing serious cardiac side effects. Some famous drugs, such as terfenadine, astemizole, grepafloxacin and cisapride, were withdrawn from the market due to their hERG inhibitory activity [33]. Recognizing hERG inhibition in an early phase is an indispensable component in drug discovery. We determined the binding affinity of the reference molecule cisapride and the four ligands for hERG channels by a traditional patch clamp technique (table 2). Two

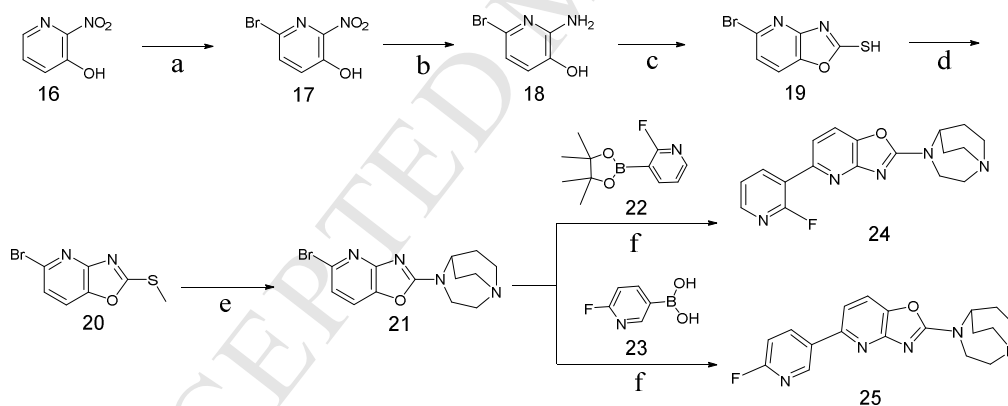
amino derivatives **5** and **14** had no significant affinity for hERG potassium channels with less than 10000 selectivity over



Scheme 1. Synthesis of meta-substitution compounds. (a) Br₂, 10% NaHSO₃, 80-85°C; (b) HNO₃, H₂SO₄; (c) Pd₂(dba)₃, BINAP, 1,4-diazabicyclo[3.2.2]nonane, t-BuONa, 1,4-dioxane, 80-85°C; (d) Fe, CH₃CH₂OH, conc. HCl, 80°C; (e) HBF₄, 0-5°C; NaNO₂; xylene, 120°C.



Scheme 2. Synthesis of ortho-substitution compounds. (a) CrO₃, H₂O, CH₃COOH, 80-85°C, 110-120°C; (b) Br₂, 80-85°C; (c) toluene, (CH₃CH₂)₃N, DPPA, t-BuOH, 110°C; (d) CH₃CN, 1 M HCl, 82°C, 1 M NaOH; (e) 30% H₂O₂, (CF₃CO)₂O, CH₂Cl₂, 0°C-RT; (f) Pd₂(dba)₃, BINAP, 1,4-diazabicyclo[3.2.2]nonane, Cs₂CO₃, toluene, 80-85°C; (g) Fe, CH₃CH₂OH, conc. HCl, 80°C; (h) HBF₄, 0-5°C; NaNO₂; xylene, 120°C.



Scheme 3. (a) CH₃ONa, RT; Br₂, 0°C; (b) Zn, NH₄Cl, 50°C; (c) CS₂, KOH, 80-85°C; (d) K₂CO₃, DMF, 0°C, CH₃I; (e) 1,4-diazabicyclo[3.2.2]nonane, (CH₃CH₂)₃N, (CH₃)₂CHOH, 100°C; (f) Cs₂CO₃, Pd(dppf)Cl₂, 1,4-dioxane, 85-90°C.

α 7-nAChRs. **15** showed modest cross-activity with hERG channels but good separation from its affinity for α 7-nAChRs. The compound **6**, however, was found to have strong hERG inhibition because of its relative low affinity for α 7-nAChRs.

Table 2
hERG inhibition (IC₅₀, nM) of cisapride and the ligands

Compd	hERG IC ₅₀ (nM) ^a	α 7-nAChRs IC ₅₀ (nM) ^b	IC ₅₀ (hERG)/ IC ₅₀ (α 7-nAChRs)
Cisapride	13.8 ± 0.76	nt ^c	nt ^c
5	2500 ± 150	0.21 ± 0.19	>10000
6	460 ± 55	20.86 ± 2.94	22
14	49700 ± 15900	0.023 ± 0.013	>10000
15	460 ± 11	6.23 ± 2.94	74

^a IC₅₀ values are the means ± SD of three experiments.

^b from an in vitro binding assay.

^c nt: not determined.

In all fluoro derivatives we synthesized, **15** had the best binding affinity and high selectivity for α 7-nAChRs. Furthermore, the radiolabeling of [¹⁸F]**15** can be accomplished by a direct nucleophilic substitution (S_NAr) with [¹⁸F]fluoride via the nitro **13** because the leaving nitro group in **13** is activated for S_NAr fluorination by the electron-withdrawing COAr on the ortho position [25, 34]. Therefore, fluoro derivative **15** was selected for labeling and further evaluation as a PET radiotracer for α 7-nAChR imaging.

2.4. Acute toxicity studies

To evaluate the safety profile of **15**, Kunming mice (half male and half female, 18-22 g, n = 60) were administered different concentrations of **15** (0.1 mL) via the tail vein, whereas the

control group was injected only with the vehicle solution. The Mice were monitored and recorded over 14 days. There was no

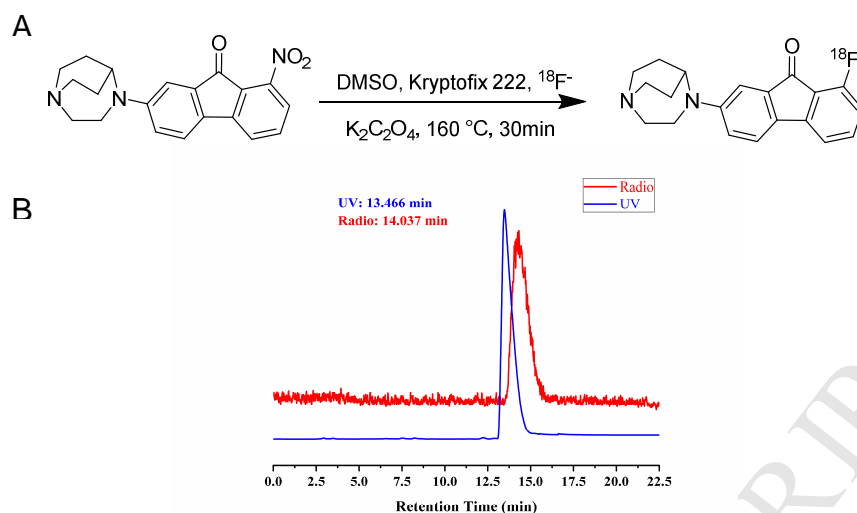


Figure 2. Radiosynthesis. (A) The radiosynthetic route of [¹⁸F]**15**. (B) HPLC chromatogram of co-injection of [¹⁸F]**15** and **15**.

morbidity or mortality in control group. In the group treated with **15**, some mice showed different degrees of convulsions, vomiting blood or death. The LD₅₀ value of **15** was 53.70 mg/kg, as calculated by the weighted probit analysis developed by Bliss, which is far greater than a PET imaging dose (μg/human), indicating that the homologous radioligand [¹⁸F]**15** is safe for use in PET imaging and is worthy of further study.

2.5. Radiochemistry

Compound **15** with high affinity and selectivity was chosen for radiolabeling with ¹⁸F in one step by treating nitro precursor **13** with ¹⁸F/K₂C₂O₄ and Kryptofix 222 in anhydrous DMSO at 160°C for 30 min (figure 2) and was purified by high-performance liquid chromatography (HPLC) in 13.1% radiochemical yield (decay not corrected) with a radiochemical purity greater than 98%. The total synthesis time was approximately 60 min. [¹⁸F]**15** was identified by comparison of its retention time with that of nonradioactive **15** via co-injection.

2.6. Octanol–water partition coefficient and in vitro stability

The ability of [¹⁸F]**15** to permeate the blood–brain barrier (BBB) was determined by estimating the partition coefficient (logP) in an *n*-octanol/phosphate buffered saline (PBS, pH = 7.4) system. The logP of [¹⁸F]**15** was 1.64 ± 0.12, which falls in a desirable range (logP = 1-3) and thus indicates increased brain uptake and decreased nonspecific binding [35, 36].

The in vitro stability of [¹⁸F]**15** in fetal bovine serum and saline was tested by measuring the radiochemistry purity via HPLC after incubation at 37°C and r.t., respectively. The radiochemistry purity in fetal bovine serum and saline after 1 h and 2 h was all greater than 98% (figure 3), indicating the high in vitro biostability of [¹⁸F]**15**.

2.7. Biodistribution in tissues and organs of mice

The biodistribution of [¹⁸F]**15** after intravenous injection was evaluated in normal Kunming mice (18-22 g, female), and the

results are summarized in table 3. [¹⁸F]**15** exhibited high initial brain uptake with 8.98 ± 0.41 %ID/g at 5 min post injection, and 11.60 ± 0.14 %ID/g, its highest uptake, at 15 min post injection. The brain_{15min}/brain_{90min} value was 3.20, a reasonable clearance rate for brain PET imaging. Among the peripheral organs, the blood uptake was low, resulting in a high brain/blood ratio of 9.57 at 30 min post injection. The lung displayed supernormal initial uptake with 70.52 ± 7.86 %ID/g at 5 min post injection but fast clearance with 20.23 ± 1.51 %ID/g at 15 min post injection and 4.99 ± 0.45 %ID/g at 90 min post injection. Notably, the bone uptake increased from 3.02 ± 0.11 %ID/g to 7.65 ± 0.52 %ID/g within 90 min post injection demonstrating the slight in vivo defluorination of [¹⁸F]**15**.

2.8. Biodistribution in brain regions of mice

The distribution of [¹⁸F]**15** in the brain of normal Kunming mice (28-32 g, female) was studied (figure 4). The highest accumulation of radioactivity was observed in the frontal cortex (9.39 ± 0.24 %ID/g), striatum (8.37 ± 0.27 %ID/g) and hippocampus (6.31 ± 0.82 %ID/g), with peak uptake at 30 min after injection, followed by a decrease. The lowest uptake was found in the cerebellum, and the radioactivity in the superior/inferior colliculus and thalamus was moderate. The distribution of [¹⁸F]**15** in the brain was consistent with the distribution of α7-nAChRs in the brain reported in the literature [20]. Moreover, the clearance rate of [¹⁸F]**15** from the cerebellum was higher than that from any other regions. Compared to the most promising ligands [¹⁸F]**A5EM** and ¹⁸F-DBT10, [¹⁸F]**15** showed similar distribution and higher peak uptake in the α7-nAChR-rich regions. The highest regional BP_{ND} value (Table 4) at 90 min (2.6 in hippocampus) was lower than that of [¹⁸F]**A5EM** (8.0 in the superior and inferior colliculus) and comparable to that of [¹⁸F]**DBT10** (3.1 in the hippocampus), probably because the binding affinity of [¹⁸F]**15** (K_i = 2.98 nM) is weaker than that of [¹⁸F]**A5EM** (K_i = 0.4 nM) and similar to that of [¹⁸F]**DBT10** (K_i = 1.3 nM); nevertheless, the highest regional BP_{ND} value of [¹⁸F]**15** is still better than that of other ligands, which in general are < 2.0.

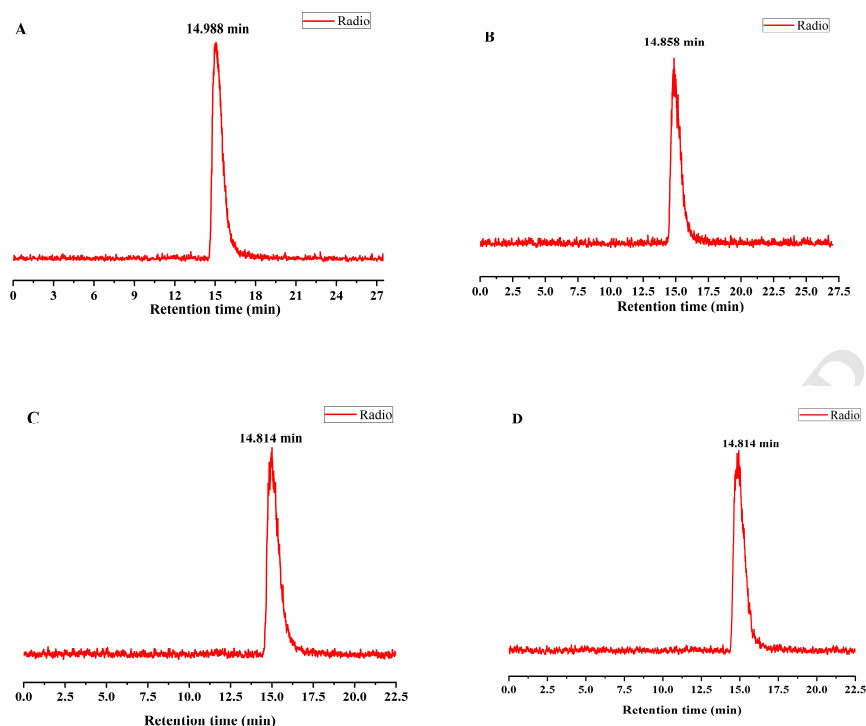


Figure 3. HPLC chromatograms of [^{18}F]15 in fetal bovine serum and saline. (A) Fetal bovine serum, 37°C, 1 h. (B) Fetal bovine serum, 37°C, 2 h. (C) Saline, RT, 1 h. (D) Saline, RT, 2 h.

Table 3

Biodistribution of [^{18}F]15 in Kunming mice (18-22 g, female)^a

organs	time (min)				
	5 min	15 min	30 min	60 min	90 min
blood	1.43 ± 0.06	1.24 ± 0.16	1.03 ± 0.07	0.68 ± 0.01	0.52 ± 0.06
brain	8.98 ± 0.41	11.60 ± 0.14	9.86 ± 0.05	5.46 ± 0.27	3.63 ± 0.25
heart	8.37 ± 0.14	4.45 ± 0.62	3.56 ± 0.31	2.19 ± 0.16	1.71 ± 0.13
liver	8.19 ± 1.19	12.28 ± 1.96	13.74 ± 1.36	9.74 ± 0.07	7.46 ± 0.19
spleen	7.72 ± 0.65	11.58 ± 0.92	8.67 ± 0.48	4.08 ± 0.38	2.97 ± 0.25
lung	70.52 ± 7.86	20.23 ± 1.51	18.30 ± 1.56	7.64 ± 0.99	4.99 ± 0.45
kidney	15.92 ± 0.24	11.54 ± 0.79	8.06 ± 0.69	4.85 ± 0.443	4.26 ± 0.19
muscle	5.51 ± 0.65	3.48 ± 0.40	2.36 ± 0.30	1.79 ± 0.06	1.32 ± 0.11
bone	3.02 ± 0.11	4.55 ± 0.68	4.84 ± 0.18	7.27 ± 1.31	7.65 ± 0.52
brain/blood	6.23	9.35	9.57	8.03	6.98

^aData are expressed as the percentage of injected dose per gram (%ID/g), mean ± SD, n = 5.

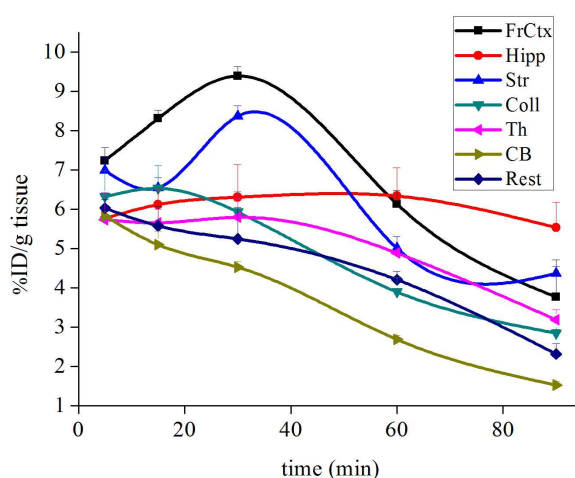


Figure 4. Biodistribution of [^{18}F]15 in the brain regions of Kunming mice (28-32 g, female). Data are expressed as the percentage of injected dose per gram (%ID/g), mean ± SD, n = 5. Abbreviations: Coll, superior and inferior colliculus; Hipp, hippocampus; FrCtx, frontal cortex; Rest, rest of the brain; Th, thalamus; Str, striatum; CB, cerebellum.

Table 4The BP_{ND} values^a of different tissues in Kunming mice (28-32 g, female) of [¹⁸F]15

tissue	BP_{ND}					
	5 min	15 min	30 min	60 min	90 min	
FrCtx	0.24	0.63	1.07	1.29	1.47	
Hipp	nt ^b	0.20	0.39	1.36	2.63	
Str	0.2	0.28	0.85	0.87	1.86	
Coll	nt ^b	0.28	0.31	0.45	0.86	
Th	nt ^b	0.11	0.28	0.82	1.10	

^a $BP_{ND} = (\text{regional uptake/cerebellum uptake}) - 1$ [37].^b nt: not determined.

Abbreviations: Coll, superior and inferior colliculus; Hipp, hippocampus; FrCtx, frontal cortex; Rest, rest of brain; Th, thalamus; Str, striatum; CB, cerebellum.

2.9. Blocking studies in CD-1 mice

To further determine the specific binding of [¹⁸F]15 to $\alpha 7$ -nAChRs over other similar receptors, blocking studies were carried out by pre-subcutaneous injection of blocking agents. $\alpha 4\beta 2$ -nAChRs, a heteromeric nAChR subtype widely expressed in the brain [38], and 5-HT₃, a receptor sharing high sequence homology with $\alpha 7$ -nAChRs [39], were the most likely receptors to cross-bind with $\alpha 7$ -nAChR ligands. Therefore, cytisine (1 mg/kg, a selective partial agonist of $\alpha 4\beta 2$ -nAChRs) and ondansetron (2 mg/kg, a selective antagonist of 5-HT₃) were pre-injected 5 min and 10 min prior to the intravenous injection of [¹⁸F]15, respectively. The mice were sacrificed at 60 min after the [¹⁸F]15 injection, and the brain tissues were harvested. As expected (figure 5), the accumulation of radiotracer in different brain regions of the blocked-group showed almost no changes compared to that in the control group, suggesting that the

binding of [¹⁸F]15 to $\alpha 7$ -nAChRs was selective over its binding to $\alpha 4\beta 2$ -nAChRs and 5-HT₃.

2.10. Micro-PET/CT imaging studies in rats

[¹⁸F]15 was evaluated in small animal PET/CT imaging studies. CD-1 rats (180-200 g, female) were injected intravenously with [¹⁸F]15 (0.3 mL, 200 μ Ci) and anesthetized with isoflurane for imaging. Axial, coronal and sagittal PET images of [¹⁸F]15 in a rat at 15, 30 and 60 min post injection are shown in figure 6. In agreement with the biodistribution results mentioned above, the highest tracer uptake in the brain was observed at 15 min post-injection, and relatively high accumulation remained at 30 min post injection. At 60 min after injection, the tracer uptake in the brain was lower but was still noticeable. The imaging results further demonstrated that [¹⁸F]15 could be a potential PET radiotracer for in vivo imaging of $\alpha 7$ -nAChRs.

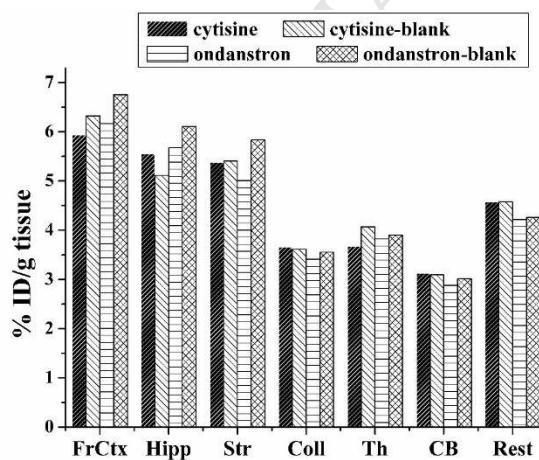


Figure 5. Blocking studies of [¹⁸F]15 accumulation in Kunming mouse brains (28-32 g, female) by pre-subcutaneous injection of cytisine (1 mg/kg) and ondansetron (2 mg/kg). Data are expressed as the percentage of injected dose per gram (%ID/g), mean \pm SD, n = 5. Abbreviations: Coll, superior and inferior colliculus; Hipp, hippocampus; FrCtx, frontal cortex; Rest, rest of brain; Th, thalamus; Str, striatum; CB, cerebellum.

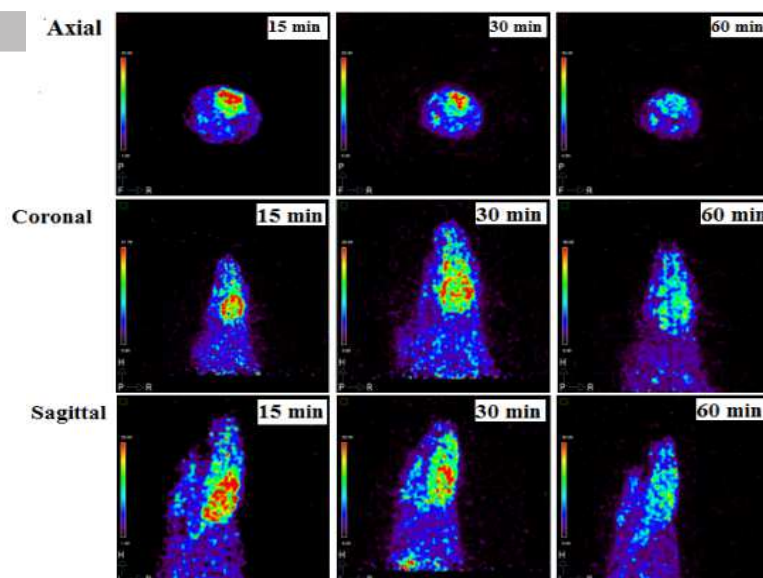


Figure 6. Micro-PET/CT images of [^{18}F]15 in CD-1 (180-200 g, female) rats.

3. Conclusion

A series of 1,4-diazobicyclo[3.2.2]nonane derivatives was prepared and evaluated as $\alpha 7$ -nAChR-targeted ligands. Five of them had high binding affinity for $\alpha 7$ -nAChR ($K_i = 0.001$ -25 nM), especially the compound **14** ($K_i = 0.0069$ nM). And four of them showed high selectivity for $\alpha 7$ -nAChRs over $\alpha 4\beta 2$ -nAChRs. In the preliminary study of agonistic activities, no strong agonist activity was found at 1 μM relative to acetylcholine at 30 μM . **5** and **14** exhibited minimal binding affinity for the hERG potassium channels, whereas **6** and **15** displayed slight cross-binding with these channels but good separation from their affinity for $\alpha 7$ -nAChRs. In acute toxicity studies, the LD_{50} of **15** (53.70 mg/kg) was far greater than a PET imaging dose ($\mu\text{g}/\text{human}$).

Fluoro derivative **15** with good binding affinity ($K_i = 2.98 \pm 1.41$ nM) was further radiolabeled with ^{18}F to afford [^{18}F]15 for PET/CT imaging. [^{18}F]15 displayed high in vitro stability and can sufficiently permeate the BBB to specially label the $\alpha 7$ -nAChRs in the brain. Furthermore, micro-PET/CT imaging in normal rats further indicated that [^{18}F]15 had obvious accumulation in the brain. Therefore, [^{18}F]15 has potential to be a suitable $\alpha 7$ -nAChR-targeted imaging radiotracer for early AD diagnosis, and further studies on this radioligand are ongoing.

4. Experiments

4.1. Materials and measurements

General procedures. All chemicals used in this work were commercial products and were utilized without further purification unless otherwise specified. ^{18}F was obtained from Peking Cancer Hospital (Beijing, China). Chemical reactions were monitored by thin-layer chromatography (TLC) using silica gel 60 GF₂₅₄ and were visualized by a UV lamp at 254 nm. Flash column chromatography was conducted on silica gel (Bonna-Agela® flash silica, 40-60 μm , 60 \AA) using an Interchim Puriflash® 4100 medium pressure preparative chromatography apparatus. NMR spectra were recorded on a Bruker Avance® III HD 400 with chemical shifts (δ) expressed in parts per million (ppm) relative to TMS as an internal standard at RT. Coupling constants (J) are reported in hertz. Multiplicity is denoted by s (singlet), d (doublet), t (triplet), quartet (q), and m (multiplet). MS spectra were recorded on a Waters Quattro Micro®

quadrupole mass spectrometer. HPLC analysis and purification were performed on a Shimadzu® LC-20AT system equipped with an SPD-20A UV detector ($\lambda = 280$ nm) and a Bioscan® flow count 3200 NaI/PMT γ -radiation scintillation detector. HPLC separations were achieved on an Inertsil® ODS-3 C18 reverse phase semi-preparative column (GL Sciences, Inc. 5 μm , 10 mm \times 250 mm) with elution using a binary gradient system at a flow rate of 4 mL/min. HPLC analysis was performed on a Venusil XBP C18(L) reverse phase analytical column (Agela Technologies, 5 μm , 150 \AA , 4.6 \times 250 mm) with elution using a binary gradient system at a flow rate of 1 mL/min. The purity of all the synthesized compounds used for biological evaluation were detected to be > 95% by an HPLC method. Radioactivity was measured on a WIZARD² 2480 automatic γ -counter (PerkinElmer, USA). SD rats (female, 180 - 200 g), normal Kunming mice (18-22 g, 28-32 g, female) and CD-1 rats (female, 180-200 g) were provided by Beijing Xinglong Animal Technology Co, Ltd., and SD mice (female, 180-200 g) were purchased from Beijing Vital River Animal Technology Co, Ltd. All mice protocols were approved by the Animal Care Committee of Beijing Normal University.

4.2. Chemistry

4.2.1. 2-Bromo-9H-fluoren-9-one (2) [40]

Br_2 (32.0 g, 0.2 mol) was added to a solution of 9H-fluoren-9-one (**1**) (30.0 g, 0.17 mol) in 100 mL of H_2O dropwise at 80-85°C over 30 min and stirred for 4 h. After complete conversion was detected by TLC, the reaction mixture was cooled to RT, quenched by the addition of 10% NaHSO_3 and then stirred for 30 min. The solid was filtered and dried to afford the corresponding compound 2-bromo-9H-fluoren-9-one (**2**) (39.1 g, 90.4%) as a yellow solid. ^1H NMR (400 MHz, CDCl_3) δ 7.76(d, $J = 1.64$ Hz, 1H), 7.66 (d, $J = 7.36$ Hz, 1H), 7.61 (dd, $J = 7.84$ Hz, 1.76 Hz, 1H), 7.51-7.50 (m, 2H), 7.39 (d, $J = 7.92$ Hz, 1H), 7.35-7.29 (m, 1H); MS ($\text{M}+\text{H}^+$): $m/z = 260.98$.

4.2.2. 2-Bromo-7-nitro-9H-fluoren-9-one (3) [40]

A suspension of 2-bromo-9H-fluoren-9-one (**2**) (0.09 mol) in H_2O (180 mL) was heated to 80-85°C and a solution of 65% HNO_3 (2.6 mol, 180 mL) and 98% H_2SO_4 (3.3 mol, 180 mL) was added dropwise. The reaction mixture was heated to reflux and continued for 4 h. After cooling to room temperature, H_2O (300 mL) was added and the mixture was filtered. The yellow cake

was washed with water (3×100 mL) and methanol (200 mL). The obtained solid was dried to provide the title product 2-bromo-7-nitro-9H-fluoren-9-one (**3**) (21.0 g, 76.4%) as a yellow solid. ¹H NMR (400 MHz, CDCl₃) δ 8.49 (s, 1H), 8.44 (d, *J* = 8.16 Hz, 1H), 7.90 (s, 1H), 7.75 (d, *J* = 7.92 Hz, 1H), 7.71 (d, *J* = 8.16 Hz, 1H), 7.55 (d, *J* = 7.92 Hz, 1H); MS (M+H⁺): *m/z* = 306.02.

4.2.3. 2-(1,4-Diazabicyclo[3.2.2]nonan-4-yl)-7-nitro-9H-fluoren-9-one (**4**) [41]

2-bromo-7-nitro-9H-fluoren-9-one (**3**) (9.0 g, 0.03 mol), Pd₂(dba)₃ (0.6 g, 0.655 mmol), BINAP (1.3 g, 2.087 mmol), t-BuONa (3.3 g, 0.0343 mol), and 1,4-diazobicyclo[3.2.2]nonane (3.0 g, 0.024 mol) were added to anhydrous 1,4-dioxane (150 mL) sequentially and the reaction mixture was stirred overnight at 80–85°C under an atmosphere of nitrogen. After cooling to room temperature, the mixture was diluted with ethyl acetate (150 mL) and filtered through Celite. The filtrate was adjusted to pH = 8.0 with 10% K₂CO₃ and then extracted with CH₂Cl₂. The combined organic layers were dried over MgSO₄, filtered and concentrated. The crude product 2-(1,4-diazabicyclo[3.2.2]nonan-4-yl)-7-nitro-9H-fluoren-9-one (**4**) was obtained as bluish violet solid (2.1 g, 20.4%) and used without further purification. ¹H NMR (400 MHz, CDCl₃) δ 7.56 (d, *J* = 7.24 Hz, 1H), 7.38 (d, *J* = 6.56 Hz, 1H), 7.34 (d, *J* = 2.8 Hz, 1H), 7.14–7.09 (m, 2H), 6.78 (d, *J* = 8.16 Hz, 1H), 4.13–4.11 (m, 1H), 3.67–3.65 (m, 1H), 3.61–3.58 (m, 1H), 3.15–3.14 (m, 4H), 3.04 (m, 2H), 2.14 (m, 2H), 1.78 (m, 2H); MS (M+H⁺): *m/z* = 350.16.

4.2.4. 2-Amino-7-(1,4-diazabicyclo[3.2.2]nonan-4-yl)-9H-fluoren-9-one (**5**) [42]

A mixture of **4** (2.1 g, 6.02 mmol), iron powder (1.7 g, 0.03 mol) in ethanol (80 mL), H₂O (54 mL) and conc. HCl (1.8 mL) was heated to 80°C for 5 h. After complete conversion was detected by TLC, the crude reaction mixture was adjusted to pH = 8.0 with a 10% solution of K₂CO₃, diluted with ethyl acetate (150 mL) and filtered through Celite. The extract was dried and concentrated under vacuum. The obtained solid was dissolved in dichloromethane and washed with water. The organic layer was dried over Na₂SO₄ and filtered, and the solvent was removed under vacuum to provide the title product 2-amino-7-(1,4-diazabicyclo[3.2.2]nonan-4-yl)-9H-fluoren-9-one (**5**) (1.5 g, 80%). ¹H NMR (400 MHz, CDCl₃) δ 7.12 (d, *J* = 8.24 Hz, 1H), 7.08 (d, *J* = 7.92 Hz, 1H), 7.01 (d, *J* = 2.44 Hz, 1H), 6.88 (d, *J* = 2.2 Hz, 1H), 6.70 (dd, *J* = 8.24 Hz, 2.52 Hz, 1H), 6.64 (dd, *J* = 7.88 Hz, 2.24 Hz, 1H), 4.01 (s, 2H), 3.51–3.48 (m, 2H), 3.13–3.06 (m, 4H), 3.01–2.94 (m, 2H), 2.12–2.05 (m, 2H), 1.75–1.67 (m, 2H); ¹³C NMR (101 MHz, CDCl₃) δ 194.18, 148.14, 144.99, 135.02, 134.79, 134.56, 132.85, 119.00, 118.94, 117.11, 110.32, 108.94, 55.59, 50.91, 45.26, 43.25, 25.50; MS (M+H⁺): *m/z* = 320.2.

4.2.5. 2-(1,4-Diaza-bicyclo[3.2.2]nonan-4-yl)-7-fluoro-9H-fluoren-9-one (**6**)

A mixture of **5** (1.9 g, 6 mmol) in HBF₄ (30 mL) was cooled to 0–5°C and stirred for 5 min. A cold solution of NaNO₂ (0.5 g, 7.2 mmol) in H₂O (15 mL) was added dropwise to the above solution and stirred for 30 min. The precipitate was filtered and washed with ethanol and tert-butyl methyl ether. The obtained diazonium tetrafluoroborate was dried and refluxed at 120°C in xylene. After complete conversion was detected, the reaction system was brought to RT and dissolved in CH₂Cl₂. The organic layer was dried over Na₂SO₄, filtered and concentrated under vacuum. The crude product was purified by flash column chromatography (CH₂Cl₂:CH₃OH = 25:1) to provide the final compound 2-(1,4-diaza-bicyclo[3.2.2]nonan-4-yl)-7-fluoro-9H-fluoren-9-one (**6**) (1.2 g, 67.3%) as a purple solid. ¹H NMR (400 MHz, CDCl₃) δ

7.24–7.19 (m, 3H), 7.05 (d, *J* = 2.28 Hz, 1H), 7.02 (dd, *J* = 8.4 Hz, 2.4 Hz, 1H), 6.74 (dd, *J* = 8.32 Hz, 2.56 Hz, 1H), 4.0437–4.0391 (m, 1H), 3.55–3.52 (m, 2H), 3.15–3.07 (m, 4H), 3.01–2.94 (m, 2H), 2.12–2.05 (m, 2H), 1.77–1.68 (m, 2H); ¹³C NMR (101 MHz, CDCl₃) δ 192.51 (d, *J* = 2.2 Hz), 162.49 (s), 160.03 (s), 148.88 (s), 140.55 (d, *J* = 2.9 Hz), 130.56 (s), 120.13 (s), 119.86 (s), 119.63 (s), 118.92 (s), 118.85 (s), 116.74 (s), 110.86 (s), 110.63 (s), 108.67 (s), 55.97 (s), 50.73 (s), 45.48 (s), 43.49 (s), 25.76 (s); ¹⁹F NMR (376 MHz, CDCl₃) δ -115.21 (s); MS (M+H⁺): *m/z* = 323.2.

4.2.6. 9-Oxo-9H-fluorene-1-carboxylic acid (**8**) [43]

A solution of CrO₃ (138.0 g, 1.38 mol) in acetic acid (80 mL) and water (120 mL) was added dropwise to a solution of fluoranthene (40.0 g, 0.2 mol) in acetic acid (500 mL) at 85°C. The solution was heated to reflux for 2 h and then poured into water (3 L). The solid precipitate was filtered and dissolved in 2 M NaOH solution (0.6 L). Conc. HCl was added, and the yellow solid obtained was filtered and dried in an oven at 100°C to provide pure 9-oxo-9H-fluorene-1-carboxylic acid (**8**) (29.5 g, 66.0%). ¹H NMR (400 MHz, CDCl₃) δ 8.20 (d, *J* = 7.84 Hz, 1H), 7.76–7.54 (m, 5H), 7.37 (t, *J* = 7.36 Hz, 1H); MS (M+H⁺): *m/z* = 225.10.

4.2.7. 7-Bromo-9-oxo-9H-fluorene-1-carboxylic acid (**9**)

The same method as described above for preparing **2** was used, and 7-bromo-9-oxo-9H-fluorene-1-carboxylic acid (**9**) was obtained as a yellow solid (19.5 g, 96.5%). ¹H NMR (400 MHz, CDCl₃) δ 8.22 (d, *J* = 7.04 Hz, 1H), 7.85 (s, 1H), 7.73–7.66 (m, 3H), 7.43 (d, *J* = 7.84 Hz, 1H).

4.2.8. Tert-butyl 2-bromo-9-oxo-9H-fluoren-8-ylcarbamate (**10**)

A solution of 7-bromo-9-oxo-9H-fluorene-1-carboxylic acid (**9**) (6 g, 19.87 mmol) in t-BuOH (10 mL) and toluene (60 mL) was treated with Et₃N (4.1 mL, 29.8 mmol) and DPPA (6.4 mL, 29.8 mmol). The reaction mixture was refluxed for 24 h and then cooled to RT. The solvent was removed under vacuum, and the crude product was purified by flash column chromatography (PE:EA = 30:1) to provide the title compound tert-butyl 2-bromo-9-oxo-9H-fluoren-8-ylcarbamate (**10**) (5.5 g, 74%). ¹H NMR (400 MHz, CDCl₃) δ 9.25 (s, 1H), 8.15 (d, *J* = 8.56 Hz, 1H), 7.72 (d, *J* = 1.56 Hz, 1H), 7.60 (dd, *J* = 7.92 Hz, 1.72 Hz, 1H), 7.43 (t, *J* = 7.56 Hz, 1H), 7.37 (d, *J* = 7.84 Hz, 1H), 7.10 (d, *J* = 7.24 Hz, 1H), 1.55 (s, 9H).

4.2.9. 1-Amino-7-bromo-9H-fluoren-9-one (**11**)

HCl (1 M, 22 mL, 21.6 mmol) was added to a stirred solution of tert-butyl 2-bromo-9-oxo-9H-fluoren-8-ylcarbamate (**10**) (808 mg, 2.16 mmol) in CH₃CN (80 mL) and heated to 80°C for 4 h. The reaction mixture was cooled to RT, adjusted to pH = 12 with 1 M NaOH and extracted with ethyl acetate. The combined organic layers were dried over Na₂SO₄, filtered and concentrated under vacuum. 1-Amino-7-bromo-9H-fluoren-9-one (**11**) was obtained as a yellow solid (500 mg, 84.5%). ¹H NMR (400 MHz, CDCl₃) δ 7.71 (d, *J* = 1.4 Hz, 1H), 7.55 (dd, *J* = 7.8 Hz, 1H), 7.35 (d, *J* = 7.9 Hz, 1H), 7.22 (t, *J* = 7.6 Hz, 1H), 6.81 (d, *J* = 7.1 Hz, 1H), 6.52 (d, *J* = 8.4 Hz, 1H), 5.54 (s, 2H); MS (M+H⁺): *m/z* = 273.99, 275.98.

4.2.10. 7-bromo-1-nitro-9H-fluoren-9-one (**12**)

A solution of trifluoroacetic anhydride (2.736 mL, 19.68 mmol) in CH₂Cl₂ (2 mL) was added dropwise to 30% H₂O₂ (16.95 mmol, 16.95 mmol) at 0°C and stirred for 1.5 h. 1-Amino-7-bromo-9H-fluoren-9-one (**11**) (500 mg, 1.824 mmol) in CH₂Cl₂ (4 mL) was added dropwise to the above mixture and warmed to RT. After 3–9 was consumed completely, the mixture was

quenched by adding water. The phases separated, and the aqueous layer was extracted three times with CH_2Cl_2 . The combined organic layers were dried over Na_2SO_4 , filtered and concentrated under vacuum. The crude product was purified by flash column chromatography (PE:EA = 10:1) to provide the title compound 7-bromo-1-nitro-9H-fluoren-9-one (**12**) (212 mg, 38.2%). ^1H NMR (400 MHz, CDCl_3) δ 7.85 (d, J = 1.6 Hz, 1H), 7.78-7.76 (m, 1H), 7.72-7.70 (m, 1H), 7.68-7.66 (m, 1H), 7.64-7.62 (m, 1H), 7.49 (d, J = 7.9 Hz, 1H). MS (M^+): m/z = 303, 305.

4.2.11. 7-(1,4-Diaza-bicyclo[3.2.2]nonan-4-yl)-1-nitro-9H-fluoren-9-one (**13**)

Under an atmosphere of nitrogen, $\text{Pd}_2(\text{dba})_3$ (0.6 g, 0.655 mmol) and BINAP (61 mg, 0.099 mmol) were stirred in anhydrous toluene (2 mL) for 15 min at 90°C . The solution was cooled to RT, and a mixture of 7-bromo-1-nitro-9H-fluoren-9-one (**12**) (100 mg, 0.329 mmol), Cs_2CO_3 (426 mg, 1.31 mmol), and 1,4-diazabicyclo[3.2.2]nonane (125 mg, 0.989 mmol) in anhydrous toluene (2 mL) was added. The reaction mixture was heated to $80\text{--}85^\circ\text{C}$ and stirred overnight. After cooling to room temperature, the mixture was quenched by adding water. The phases separated and the aqueous layer extracted three times with CH_2Cl_2 . The combined organic layers were dried over Na_2SO_4 , filtered and concentrated under vacuum. The crude product was purified by flash column chromatography (CH_2Cl_2 : CH_3OH = 20:1) to provide the title compound 7-(1,4-diaza-bicyclo[3.2.2]nonan-4-yl)-1-nitro-9H-fluoren-9-one (**13**) (48 mg, 41.8%). ^1H NMR (400 MHz, CDCl_3) δ 7.52-7.49 (m, 2H), 7.36 (d, J = 7.9 Hz, 2H), 7.10 (s, 1H), 6.82 (t, J = 7.6 Hz, 1H), 4.13 (s, 1H), 3.63-3.62 (m, 2H), 3.18-3.04 (m, 6H), 2.31 (s, 2H), 1.83-1.82 (m, 2H); MS ($\text{M}+\text{H}^+$): m/z = 350.37.

4.2.12. 7-(1,4-Diaza-bicyclo[3.2.2]nonan-4-yl)-1-amino-9H-fluoren-9-one (**14**)

The same method as described above for preparing **5** was used, and 7-(1,4-diaza-bicyclo[3.2.2]nonan-4-yl)-1-amino-9H-fluoren-9-one (**14**) was obtained as a purple solid (1.5 g, 80%). ^1H NMR (400 MHz, CDCl_3) δ 7.30 (d, J = 8.28 Hz, 1H), 7.16-7.12 (m, 1H), 7.06 (d, J = 2.48 Hz, 1H), 6.75 (dd, J = 8.28 Hz, 2.52 Hz, 1H), 6.67 (d, J = 7.04 Hz, 1H), 6.35 (d, J = 8.28 Hz, 1H), 5.43 (s, 2H), 4.10 (s, 1H), 3.58 (t, J = 5.48 Hz, 2H), 3.19-3.13 (m, 3H), 3.07-3.00 (m, 2H), 2.14-2.11 (m, 2H), 1.80-1.74 (m, 3H); ^{13}C NMR (100 MHz, CDCl_3) δ 195.66 (s), 150.20 (s), 147.18 (s), 137.02-136.73 (m), 136.37 (s), 131.22 (s), 121.42 (s), 116.55 (s), 115.39 (s), 108.58 (s), 108.48 (s), 57.06 (s), 51.87 (s), 46.56 (s), 44.64 (s), 26.91 (s); MS ($\text{M}+\text{H}^+$): m/z = 320.16.

4.2.13. 7-(1,4-Diaza-bicyclo[3.2.2]nonan-4-yl)-1-fluoro-9H-fluoren-9-one (**15**)

The same reaction as described above for preparing **6** was used, and 7-(1,4-diaza-bicyclo[3.2.2]nonan-4-yl)-1-fluoro-9H-fluoren-9-one (**15**) was obtained as a purple solid (446 mg, 34.0%). ^1H NMR (400 MHz, CDCl_3) δ 7.39-7.34 (m, 1H), 7.32 (d, J = 8.36 Hz, 1H), 7.11 (d, J = 7.36 Hz, 1H), 7.09 (d, J = 2.48 Hz, 1H), 6.80-6.74 (m, 2H), 4.10 (s, 1H), 3.60 (t, J = 5.76 Hz, 2H), 3.19-3.12 (m, 4H), 3.05-2.99 (m, 2H), 2.15-2.10 (m, 2H), 1.82-1.73 (m, 2H); ^{13}C NMR (101 MHz, CDCl_3) δ 191.17 (s), 158.08 (s), 150.54 (s), 137.22 (s), 137.14 (s), 135.82 (s), 130.97 (s), 121.76 (s), 117.27 (s), 115.33 (s), 115.12 (s), 114.98 (s), 109.26 (s), 56.85 (s), 51.62 (s), 46.36 (s), 44.39 (s), 29.70 (s), 26.65 (s); ^{19}F NMR (376 MHz, CDCl_3) δ -114.11 (s); MS ($\text{M}+\text{H}^+$): m/z = 323.2.

4.2.14. 2-nitropyridin-3-ol (**17**)

Under an atmosphere of nitrogen, a solution of CH_3ONa (2.89 g, 53.5 mmol) in CH_3OH (15 mL) was added dropwise to a

solution of 2-nitropyridin-3-ol (**16**) (5 g, 35.7 mmol) in CH_3OH (50 mL) and the mixture was stirred at RT for 30 min. After the reaction system cooling to 0°C , Br_2 (6.3 g, 39.4 mmol) was added dropwise with stirring. After **16** was consumed, the mixture was quenched by adding a solution of 10% Na_2SO_3 and then cooled to -15°C . Yellow solid was precipitated, filtered and washed with cold CH_3OH . The title compound was obtained as a yellow solid (4.2 g, 53%). ^1H NMR (400 MHz, DMSO) δ 7.85 (d, J = 8.64 Hz, 1H), 7.66 (d, J = 8.64 Hz, 1H); MS ($\text{M}+\text{H}^+$): m/z = 216.97.

4.2.15. 6-bromo-2-nitropyridin-3-ol (**18**)

Under an atmosphere of nitrogen, zinc powder (1.5 g, 22.9 mmol) and NH_4Cl (1.5 g, 22.9 mmol) were added to the solution of 2-nitropyridin-3-ol (**17**) (1 g, 4.6 mmol) in $\text{C}_2\text{H}_5\text{OH}$ (20 mL). The reaction was heated to 50°C and stirred for 16 h. The crude reaction mixture was filtered and purified by flash column chromatography (PE:EA = 5:1) to provide the title compound 6-bromo-2-nitropyridin-3-ol (**18**) (524 mg, 60%). ^1H NMR (400 MHz, DMSO) δ 9.70 (s, 1H), 6.74 (d, J = 7.8 Hz, 1H), 6.49 (d, J = 7.8 Hz, 1H), 5.91 (s, 1H); MS ($\text{M}+\text{H}^+$): m/z = 188.99.

4.2.16. 5-bromooxazolo[4,5-b]pyridine-2-thiol (**20**)

KOH (191 mg, 4.76 mmol) was added to a stirred mixture of 6-bromo-2-nitropyridin-3-ol (**18**) (0.3 g, 1.59 mmol) in $\text{C}_2\text{H}_5\text{OH}$ (10 mL) under an argon atmosphere. Carbon disulfide (2.42 g, 31.7 mmol) was added and the reaction mixture was heated to reflux for 16 h. The reaction mixture was evaporated to dryness, and water (250 mL) was added followed by HCl until the pH was ~ 3 . The formed precipitate was separated by filtration, washed with H_2O , and dried to provide the crude product **19** (0.26 g).

K_2CO_3 was added to a stirred mixture of the above product (0.26 g, 1.13 mmol) in DMF (10 mL) under argon. Then methyl iodide (1.24 mmol) was added dropwise at 0°C . The mixture was stirred at RT for 2 h and evaporated. H_2O (60 mL) and ethyl acetate (20 mL) were added to the residue, and the mixture was stirred for 5 min. The organic layer was separated, and the aqueous layer was extracted with ethyl acetate (3×200 mL). The combined organic layers were dried over Na_2SO_4 and evaporated to provide the title compound 5-bromooxazolo[4,5-b]pyridine-2-thiol (**20**) (180 mg, 65%). ^1H NMR (400 MHz, DMSO) δ 8.06 (d, J = 8.4 Hz, 1H), 7.55 (d, J = 8.4 Hz, 1H), 2.79 (s, 3H); MS ($\text{M}+\text{H}^+$): m/z = 246.93.

4.2.17. 5-bromo-2-(methylthio)oxazolo[4,5-b]pyridine (**21**)

1,4-Diazabicyclo[3.2.2]nonane (200 mg, 1.58 mmol) was added to a solution of 5-bromooxazolo[4,5-b]pyridine-2-thiol (**20**) (466 mg, 1.9 mmol) and NEt_3 (321 mg, 3.17 mmol) in *i*-PrOH (10 mL). The mixture was placed in an oil bath at 100°C and the solvent was evaporated. The mixture was allowed to stir neat at 90°C overnight. Upon cooling to RT, the mixture was purified by flash column chromatography (EA) to provide the title compound 5-bromo-2-(methylthio)oxazolo[4,5-b]pyridine (**21**) (250 mg, 48.8%). ^1H NMR (400 MHz, DMSO) δ 7.68 (d, J = 8.12 Hz, 1H), 7.15 (d, J = 8.12 Hz, 1H), 4.43-4.42 (m, 1H), 3.90 (t, J = 5.56 Hz, 2H), 3.09 (t, J = 5.76 Hz, 2H), 3.04-2.95 (m, 4H), 2.10-2.07 (m, 2H), 1.84-1.76 (m, 2H); MS ($\text{M}+\text{H}^+$): m/z = 323.905.

4.2.18. 2-(1,4-diazabicyclo[3.2.2]nonan-4-yl)-5-(2-fluoropyridin-3-yl)oxazolo[4,5-b]pyridine (**24**)

Under an atmosphere of nitrogen, Cs_2CO_3 (303 mg, 0.93 mmol) and $\text{Pd}(\text{dppf})\text{Cl}_2$ (45 mg, 0.062 mmol) were added to a solution of 5-bromo-2-(methylthio)oxazolo[4,5-b]pyridine (**21**) (100 mg, 0.31 mmol), 2-fluoro-3-(4,4,5,5-tetramethyl-1,3,2-dioxaborolan-2-yl)pyridine (**22**) (70 mg, 0.314 mmol) in 1,4-dioxane and heated to $85\text{--}90^\circ\text{C}$. After complete conversion was detected, the residue was purified by flash column chromatography (PE:EA =

10:1) to provide the title compound 2-(1,4-diazabicyclo[3.2.2]nonan-4-yl)-5-(2-fluoropyridin-3-yl)oxazolo[4,5-b]pyridine (**24**) as yellow solid (89.4 mg, 85%). ¹H NMR(400 MHz, CDCl₃) δ 8.72 (td, *J* = 8.82 Hz, 2 Hz, 1H), 8.18 (dt, *J* = 1.76 Hz, 4.32 Hz, 1H), 7.61 (dd, *J* = 8.24 Hz, 1.32 Hz, 1H), 7.49 (d, *J* = 8.2 Hz, 1H), 7.30 (td, *J* = 5.94 Hz, 2.04 Hz, 1H), 4.61 (s, 1H), 3.99(m, 2H), 3.21-3.13 (m, 4H), 3.06-2.99(m, 2H), 2.18-2.16 (m, 2H), 1.88-1.80 (m, 2H); ¹³C NMR (100 MHz, CDCl₃) δ 163.54, 161.83, 159.45, 158.78, 146.72, 146.02, 141.72, 141.05, 122.63, 122.37, 122.01, 116.37, 114.92, 56.96, 50.73, 46.32, 44.33, 26.82; MS (M+H⁺): *m/z* = 340.15.

4.2.19. 2-(1,4-diazabicyclo[3.2.2]nonan-4-yl)-5-(6-fluoropyridin-3-yl)oxazolo[4,5-b]pyridine (**25**)

The same method as described above for preparing **24** was used, and 2-(1,4-diazabicyclo[3.2.2]nonan-4-yl)-5-(6-fluoropyridin-3-yl)oxazolo[4,5-b]pyridine (**25**) was obtained as yellow solid (53 mg, 50%). ¹H NMR (400 MHz, CDCl₃) δ 8.80 (d, *J* = 2.32 Hz, 1H), 8.52 (td, *J* = 7.8 Hz, 2.52 Hz, 1H), 7.50 (d, *J* = 8.16 Hz, 1H), 7.35 (d, *J* = 8.12 Hz, 1H), 6.99 (dd, *J* = 8.52 Hz, 2.8 Hz, 1H), 4.65 (s, 1H), 4.03 (t, *J* = 5.36 Hz, 2H), 3.25-3.19 (m, 4H), 3.10-3.04 (m, 2H), 2.22 (m, 2H), 1.93-1.86 (m, 2H); ¹³C NMR (100 MHz, CDCl₃) δ 164.88, 163.48, 162.49, 158.88, 149.03, 145.90, 141.07, 139.96, 133.43, 115.37, 112.24, 109.51, 109.14, 55.83, 50.57, 46.30, 26.43, 8.70; MS(M+H⁺): *m/z* = 340.16.

4.3. Radiolabeling

[¹⁸F]fluoride trapped on a QMA cartridge was transferred into a high-pressure digestion tank with a solution of Kryptofix 222/K₂C₂O₄ (a mixture of 15 mg Kryptofix 222 in 0.7 mL CH₃CN and 2 mg K₂C₂O₄ in 0.3 mL H₂O). The solvent was removed at 100°C under a stream of nitrogen gas. The residue was azeotropically dried with 0.5 mL of anhydrous CH₃CN three times at 100°C under a stream of nitrogen gas. Nitro precursor **13** (2 mg) in anhydrous DMSO (0.3 mL) was added to the above mentioned high-pressure digestion tank and heated to 160°C for 30 min. The mixture was diluted with water (2×10 mL) and passed through a Sep-Pak C18 cartridge. After washing the column with additional water (10 mL), the crude product was eluted with CH₃CN (2 mL), and the solvent was removed under vacuum. The residue was dissolved in CH₃CN and purified by HPLC (mobile phase: CH₃CN/H₂O (0.2% NH₄OAc) = 28/72, flow rate = 4 mL/min, λ = 280 nm). Identification was achieved by analytical HPLC (mobile phase: CH₃CN/H₂O (0.2% NH₄OAc) = 28/72, flow rate = 1 mL/min, λ = 280 nm). The total synthesis time was approximately 60 min. The radiochemical yield was 13.1% (decay not corrected), and the radiochemical purity was greater than 98%.

4.4. In vitro binding assay

Preparation of rat membranes: SD rats (female, 180 - 200 g) were used for the experiment. After the rats were sacrificed by decapitation, the brains were rapidly removed from the skulls and dissected on ice. The cerebral cortexes (rich in α7 nAChRs) were collected, homogenized at 4°C in 15 volumes of ice-cold Tris-HCl buffer (50 mM Tris, 120 mM NaCl, 5 mM KCl, 2 mM CaCl₂, 1 mM MgCl₂, pH = 7.4) and centrifuged at 48000 g for 20 min at 4°C. The supernatant was discarded, and the pellets were resuspended, homogenized and centrifuged as above three times. Subsequently, the pellets were resuspended into 10 volumes of buffer and kept at -80°C. Protein concentrations were measured using the method of Lowry et al. [44]

Ligand-binding assay:

α7-nAChR assay: the saturation binding assay was conducted using the membranes (1.5 mg) prepared above incubated in Tris-HCl buffer at 37°C for 150 min with different concentrations of [¹²⁵I]α-bungarotoxin (10 μL) in a final volume of 500 μL. Nonspecific binding was estimated by adding α-bungarotoxin (2 μM, 100 μL). The binding was terminated by rapid vacuum filtration through glass fiber filters (Whatman GF/B, presoaked in 0.5% (v/v) polyethyleneimine for 150 min) using an Mp-48T cell harvester (Brandel, Gaithersburg, MD), and the filters were washed with ice-cold Tris-HCl buffer 3 times. The radioactivity retained on the filters was counted using an automatic γ-counter. The reference ligand **MLA** and the synthesized compounds were evaluated in the presence of [¹²⁵I]α-bungarotoxin (0.4 nM). These assays were performed independently in triplicate. Binding assay results were analyzed using GraphPad Prism 5.0 software, and the Ki values were calculated using the Cheng-Prusoff equation.

α4β2-nAChRs assay: the affinity of the compounds for α4β2-nAChRs was carried out using a modification method described above. In brief, [³H]cytisine (1nM) as the radioligand competed with test compounds. Nonspecific binding was measured by adding 1μM cytosine. Incubation and filtration were performed as described above. The samples were counted in a liquid scintillation counter and the data was analyzed using the method mentioned above.

4.5. Patch clamp electrophysiology

Agonistic effects were assessed by a manual patch clamp technique performed commercially by Beijing Ice Bioscience NIC.

4.6. hERG assay

The hERG inhibitory activity of the four derivatives was measured by a traditional patch clamp technique performed commercially by Beijing Ice Bioscience NIC. In general, HEK293 cells stably expressing hERG potassium channels were routinely grown at 37°C under a 5% CO₂ atmosphere in Dulbecco's modified eagle's medium/nutrient mixture (DMEM) supplemented with 10% heat-inactivated fetal bovine serum and 0.2 mg/mL geneticin. After culture, TrypLE™Express solution was used to separate the cells, then 3×10⁵ cells were spread onto a cover glass, and the cell electrophysiological activity was detected after incubation for 18 h in a 24 well plate. The ligands were evaluated until the hERG channel currents were stable. All of the experiments were performed independently 3 times.

4.7. Acute toxicity assay

Kunming mice (half male and half female, 18-20 g, n = 60) were fed for 3 days, and after 12 h of fasting (food but not water was withheld), the mice were weighed and randomly divided into 6 groups. Every mouse was injected with different concentrations of **15** (0.1 mL) via the tail vein, and the control groups were injected only with the vehicle solution. The conditions of the mice, including behavioral activities, food intake, changes in body weight, and signs of toxicity or death, were observed over a span of 14 days. The LD₅₀ value was obtained by the weighted probit analysis developed by Bliss.

4.8. Partition coefficient determination

The partition coefficient of [¹⁸F]**15** was determined by measuring the distribution of the radioligand in n-octanol and phosphate buffered saline (PBS). [¹⁸F]**15** (10 μCi) dissolved in 0.1 mL of saline was added to a centrifuge tube, to which 0.8 mL of PBS saturated with n-octanol and 0.9 mL n-octanol saturated

with PBS were added. The tube was vortexed for 1.0 min, followed by centrifugation for 5 min at 7000 rpm. Then, two samples (0.1 mL each) from each phase were counted in an automatic γ -counter. The partition coefficient was expressed as log P which was calculated using the following equation: $\log P = \log(\text{counts (n-octanol)}/\text{counts (PBS)})$. Samples (0.45 mL) from the n-octanol layer were repartitioned until consistent distribution coefficient values were obtained. The measurement was repeated three times in triplicate.

4.9. *In vitro stability studies*

In vitro stability in fetal bovine serum and saline: [^{18}F]**15** (10 μCi) was incubated in fetal bovine serum (100 μL) and saline (100 μL) at 37°C and RT, respectively. The incubation mixtures were sampled at 60 min and 120 min and loaded onto the HPLC system for analysis. Specifically, the fetal bovine serum sample was treated using the following procedure: after incubating, the serum protein was precipitated by adding acetonitrile (200 μL), and the sample was centrifuged for 5 min at 7000 rpm. The supernatant was filtered through an organic Millipore filter (0.22 μm) for HPLC analysis.

4.10. *Biodistribution in tissues and organs in mice*

Normal Kunming mice (female, 18-22 g, $n = 5$) were injected with [^{18}F]**15** (10 μCi , in saline (0.1 mL) containing 5% DMSO) via the tail vein and sacrificed by decapitation at 5, 15, 30, 60 and 90 min post-injection. The tissue and organs of interest were removed, weighed and counted by an automatic γ -counter. The percent dose per gram of wet tissue (%ID/g) was calculated by comparison of the tissue counts with suitably diluted aliquots of the injected material. The values were expressed as the mean \pm SD ($n = 5$).

4.11. *Biodistribution in the brain regions of mice*

Normal Kunming mice (female, 28-32 g, $n = 5$) were injected with [^{18}F]**15** (10 μCi , in saline (0.1 mL) containing 5% DMSO) via the tail vein and sacrificed by cervical dislocation at 5, 15, 30, 60 and 90 min post-injection. The brains were rapidly removed from the skulls and then dissected on ice into the cortex, hippocampus, striatum, superior and inferior colliculus, thalamus, cerebellum and rest of the brain. The brain regions were weighed and the radioactivity was determined with an automatic γ -counter. The data was analyzed as described as above.

4.12. *Drug inhibition studies*

Blocking studies were carried out by pre-subcutaneous injection of normal Kunming mice (female, 28-32 g, $n = 5$) with blocking agents. Cytisine (1 mg/kg, 0.1 mL saline/propylene glyco (v/v = 1/1)) and ondansetron (2 mg/kg, 0.1 mL saline/DMSO (v/v = 5/1)) were injected 5 min and 10 min prior to the intravenous injection of [^{18}F]**15** (0.1 mL, 60 μCi), respectively. Control groups were injected with the vehicle solution (0.1 mL). At 60 min after the [^{18}F]**15** injection, the brain was treated according to the procedure for determining biodistribution in various brain regions of mice.

4.13. *Micro-PET/CT imaging*

CD-1 rats (female, 180-200 g) were injected intravenously with [^{18}F]**15** (0.3 mL, 200 μCi), anesthetized with isoflurane (3% isoflurane for preparation and 1% isoflurane during scanning) and fixed on the bed of a micro-PET/CT scanner in the prone

position. Images were acquired at 15, 30 and 60 min post-injection.

Compliance with ethical standards

All protocols requiring the use of mice were approved by the Animal Care Committee of Beijing Normal University.

Author contributions

[†]Shuxia Wang and Yu Fang contributed equally to this work.

Conflicts of interest

The authors declare no conflict of interest.

Acknowledgments

The work was financially supported by the National Major Scientific and Technological Special Project for "Significant New Drugs Development" (Grant Nos. 2014ZX09507007-001 and 2014ZX09507007-003), the National Science and Technology Support Program (Grant No. 2014BAA03B03) and the National Natural Science Foundation of China (Grant Nos. 21371026). We also thank the Nuclear Medicine Department of Peking Cancer Hospital (Beijing, China) for providing the fluoride-18 nuclide and allowing us to use the micro-PET/CT scanner.

Appendix A. Supplementary data

Data analysis of the patch clamp electrophysiological assay, and acute toxicity assay, and ^1H NMR, ^{13}C NMR and MS spectra are listed in the supporting information.

References

- [1] R. Brookmeyer, S. Gray, C. Kawas, Projections of Alzheimer's disease in the United States and the public health impact of delaying disease onset, *Am. J. Public Health* 88 (1998) 1337-1342.
- [2] T.L. Wallace, R.H.P. Porter, Targeting the nicotinic alpha7 acetylcholine receptor to enhance cognition in disease, *Biochem. Pharmacol.* 82 (2011) 891-903.
- [3] M.R. Picciotto, B.J. Caldarone, S.L. King, V. Zachariou, Nicotinic receptors in the brain: Links between molecular biology and behavior, *Neuropsychopharmacology* 22 (2000) 451-465.
- [4] J.A. Dani, D. Bertrand, Nicotinic acetylcholine receptors and nicotinic cholinergic mechanisms of the central nervous system, *Annu. Rev. Pharmacol. Toxicol.* 47 (2007) 699-729.
- [5] C. Gotti, F. Clementi, Neuronal nicotinic receptors: from structure to pathology, *Prog. Neurobiol.*, 74 (2004) 363-396.
- [6] M.J.C. Marks, Allan C., Characterization of nicotine binding in mouse brain and comparison with the binding of α -bungarotoxin and quinuclidinyl benzilate, *Mol. Pharmacol.* 22 (1982) 554-564.
- [7] S. Couturier, D. Bertrand, J.M. Matter, M.C. Hernandez, S. Bertrand, N. Millar, S. Valera, T. Barkas, M. Ballivet, A Neuronal Nicotinic Acetylcholine-Receptor Subunit (Alpha-7) Is Developmentally Regulated and Forms a Homooligomeric Channel Blocked by Alpha-Btx, *Neuron* 5 (1990) 847-856.
- [8] P. Seguela, J. Wadiche, K. Dineley-Miller, J.A. Dani, J.W. Patrick, Molecular cloning, functional properties, and distribution of rat brain alpha 7: a nicotinic cation channel highly permeable to calcium, *J Neurosci* 13 (1993) 596-604.
- [9] M. Oz, D.E. Lorke, K.H. Yang, G. Petroianu, On the interaction of beta-amyloid peptides and alpha7-nicotinic acetylcholine receptors in Alzheimer's disease, *Current Alzheimer research* 10 (2013) 618-630.
- [10] P. Davies, S. Feisullin, Postmortem stability of alpha-bungarotoxin binding sites in mouse and human brain, *Brain Res* 216 (1981) 449-454.
- [11] A. Wevers, L. Monteggia, S. Nowacki, W. Bloch, U. Schutz, J. Lindstrom, E.F. Pereira, H. Eisenberg, E. Giacobini, R.A. de Vos, E.N. Steur, A. Maelicke, E.X. Albuquerque, H. Schroder, Expression of

- nicotinic acetylcholine receptor subunits in the cerebral cortex in Alzheimer's disease: histotopographical correlation with amyloid plaques and hyperphosphorylated-tau protein, *Eur J Neurosci* 11 (1999) 2551-2565.
- [12] M.S.H. Thomsen, Henrik H.; Timmerman, Daniel B.; Mikkelsen, Jens D., Cognitive improvement by activation of $\alpha 7$ nicotinic acetylcholine receptors: from animal models to human pathophysiology, *Curr. Pharm. Des.* 16 (2010) 323-343.
- [13] a.K.H. Jun Toyohara, $\alpha 7$ Nicotinic receptor agonists: potential therapeutic drugs for treatment of cognitive impairments in schizophrenia and Alzheimer's disease, *The Open Medicinal Chemistry Journal* 4 (2010) 37-56.
- [14] A.A. Mazurov, J.D. Speake, D. Yohannes, Discovery and development of alpha7 nicotinic acetylcholine receptor modulators, *J. Med. Chem.* 54 (2011) 7943-7961.
- [15] C.A. Briggs, D.J. Anderson, J.D. Brioni, J.J. Buccafusco, M.J. Buckley, J.E. Campbell, M.W. Decker, D. Donnelly-Roberts, R.L. Elliott, M. Gopalakrishnan, M.W. Holladay, Y.H. Hui, W.J. Jackson, D.J. Kim, K.C. Marsh, A. O'Neill, M.A. Prendergast, K.B. Ryther, J.P. Sullivan, S.P. Arneric, Functional characterization of the novel neuronal nicotinic acetylcholine receptor ligand GTS-21 in vitro and in vivo, *Pharmacol. Biochem. Behav.* 57 (1997) 231-241.
- [16] G. Mullen, J. Napier, M. Balestra, T. DeCory, G. Hale, J. Macor, R. Mack, J. Loch, E. Wu, A. Kover, P. Verhoest, A. Sampognaro, E. Phillips, Y.Y. Zhu, R. Murray, R. Griffith, J. Blosser, D. Gurley, A. Machulskis, J. Zongrone, A. Rosen, J. Gordon, (-)-spiro[1-azabicyclo[2.2.2]octane-3,5'-oxazolidin-2'-one], a conformationally restricted analogue of acetylcholine, is a highly selective full agonist at the alpha 7 nicotinic acetylcholine receptor, *J. Med. Chem.* 43 (2000) 4045-4050.
- [17] B. Biton, O.E. Bergis, F. Galli, A. Nedelec, A.W. Lochead, S. Jegham, D. Godet, C. Lanneau, R. Santamaria, F. Chesney, J. Leonardon, P. Granger, M.W. Debono, G.A. Bohme, F. Sgard, F. Besnard, D. Graham, A. Coste, A. Oblin, O. Curet, X. Vige, C. Voltz, L. Rouquier, J. Souilhac, V. Santucci, C. Gueudet, D. Francon, R. Steinberg, G. Griebel, F. Oury-Donat, P. George, P. Avenet, B. Scatton, SSR180711, a novel selective alpha7 nicotinic receptor partial agonist: (1) binding and functional profile, *Neuropsychopharmacology* 32 (2007) 1-16.
- [18] A.A. Mazurov, D.C. Kombo, T.A. Hauser, L. Miao, G. Dull, J.F. Genus, N.B. Fedorov, L. Benson, S. Sidach, Y. Xiao, P.S. Hammond, J.W. James, C.H. Miller, D. Yohannes, Discovery of (2S,3R)-N-[2-(pyridin-3-ylmethyl)-1-azabicyclo[2.2.2]oct-3-yl]benzo[b]furan-2-carboxamide (TC-5619), a selective alpha7 nicotinic acetylcholine receptor agonist, for the treatment of cognitive disorders, *J. Med. Chem.* 55 (2012) 9793-9809.
- [19] J. Cook, F.C. Zusi, I.M. McDonald, D. King, M.D. Hill, C. Iwuagwu, R.A. Mate, H.Q. Fang, R.L. Zhao, B. Wang, J. Cutrone, B.Q. Ma, Q. Gao, R.J. Knox, M. Matchett, L. Gallagher, M. Ferrante, D. Post-Munson, T. Molski, A. Easton, R. Miller, K. Jones, S. Digavalli, F. Healy, K. Lentz, Y. Benitex, W. Clarke, J. Natale, J.A. Siuciak, N. Lodge, R. Zaczek, R. Denton, D. Morgan, L.J. Bristow, J.E. Macor, R.E. Olson, Design and Synthesis of a New Series of 4-Heteroarylamino-1'-azaspiro[oxazole-5,3'-bicyclo[2.2.2]octanes as alpha 7 Nicotinic Receptor Agonists. 1. Development of Pharmacophore and Early Structure - Activity Relationship, *J. Med. Chem.* 59 (2016) 11171-11181.
- [20] J. Toyohara, J. Wu, K. Hashimoto, Recent development of radioligands for imaging alpha7 nicotinic acetylcholine receptors in the brain, *Curr. Top. Med. Chem.* 10 (2010) 1544-1557.
- [21] P. Brust, D. Peters, W. Deuther-Conrad, Development of radioligands for the imaging of alpha7 nicotinic acetylcholine receptors with positron emission tomography, *Curr. Drug Targets* 13 (2012) 594-601.
- [22] M.G. Pomper, E. Phillips, H. Fan, D.J. McCarthy, R.A. Keith, J.C. Gordon, U. Scheffel, R.F. Dannals, J.L. Musachio, Synthesis and biodistribution of radiolabeled alpha(7) nicotinic acetylcholine receptor ligands, *J. Nucl. Med.* 46 (2005) 326-334.
- [23] K.N. Hashimoto, S.; Ohba, H.; Matsuo, M.; Kobashi., M.I. T.; Takahagi, M.; Kitashoji, T.; Tsukada, H. , [11C]CHIBA-1001 as a novel PET ligand for alpha7 nicotinic receptors in the brain: a PET study in conscious monkeys, *PLoS One* 3 (2008) e3231.
- [24] W.F. Deuther-Conrad, S.; Hiller, A.; Becker, G.; Cumming, P.; Xiong, G.; Funke, U.; Sabri, O.; Peters, D.; Brust, P., Assessment of alpha7 nicotinic acetylcholine receptor availability in juvenile pig brain with [18F]NS10743, *Eur. J. Nucl. Med. Mol. Imaging* 38 (2011).
- [25] Y. Gao, K.J. Kellar, R.P. Yasuda, T. Tran, Y. Xiao, R.F. Dannals, A.G. Horti, Derivatives of dibenzothioephene for positron emission tomography imaging of alpha7-nicotinic acetylcholine receptors, *J. Med. Chem.* 56 (2013) 7574-7589.
- [26] D.F. Wong, H. Kuwabara, M. Pomper, D.P. Holt, J.R. Brasic, N. George, B. Frolov, W. Willis, Y. Gao, H. Valentine, A. Nandi, L. Gapasin, R.F. Dannals, A.G. Horti, Human brain imaging of alpha7 nAChR with [(18)F]ASEM: a new PET radiotracer for neuropsychiatry and determination of drug occupancy, *Mol. Imaging Biol.* 16 (2014) 730-738.
- [27] A.T.L. Hillmer, Songye; Zheng, Ming-Qiang; Scheunemann, Matthias; Lin, Shu-fei; Nabulsi, Nabeel; Holden, Daniel; Pracitto, Richard; Labaree, David; Ropchan, Jim; Teodoro, Rodrigo; Deuther-Conrad, Winnie; Esterlis, Irina; Cosgrove, Kelly P.; Brust, Peter; Carson, Richard E.; Huang, Yiyun, PET imaging of $\alpha 7$ nicotinic acetylcholine receptors: a comparative study of [18F]ASEM and [18F]DBT-10 in nonhuman primates, and further evaluation of [18F]ASEM in humans, *Eur. J. Nucl. Med. Mol. Imaging* 44 (2017) 1042-1050.
- [28] C.J. O'Donnell, B.N. Rogers, B.S. Bronk, D.K. Bryce, J.W. Coe, K.K. Cook, A.J. Duplantier, E. Evrard, M. Hajos, W.E. Hoffmann, R.S. Hurst, N. Maklad, R.J. Mather, S. McLean, F.M. Nedza, B.T. O'Neill, L. Peng, W. Qian, M.M. Rottas, S.B. Sands, A.W. Schmidt, A.V. Shrikhande, D.K. Spracklin, D.F. Wong, A. Zhang, L. Zhang, Discovery of 4-(5-methyloxazo[4,5-b]pyridin-2-yl)-1,4-diazabicyclo[3.2.2]nonane (CP-810,123), a novel alpha 7 nicotinic acetylcholine receptor agonist for the treatment of cognitive disorders in schizophrenia: synthesis, SAR development, and in vivo efficacy in cognition models, *J. Med. Chem.* 53 (2010) 1222-1237.
- [29] M.R. Schrimpf, K.B. Sippy, C.A. Briggs, D.J. Anderson, T. Li, J. Ji, J.M. Frost, C.S. Surowy, W.H. Bunnelle, M. Gopalakrishnan, M.D. Meyer, SAR of alpha7 nicotinic receptor agonists derived from tilorone: exploration of a novel nicotinic pharmacophore, *Bioorg. Med. Chem. Lett.* 22 (2012) 1633-1638.
- [30] A.Q. Wu, X. Li, Q.Q. Xue, Y.J. Liu, X. Lu, X. Yan, H.B. Zhang, Radio synthesis and in vivo evaluation of two alpha 7 nAChRs radioligands: [1-125]CAIPE and [I-125]IPPU, *J. Radioanal. Nucl. Chem.* 307 (2016) 1345-1351.
- [31] W. Huan, W. Aiqin, L. Jianping, X. Qianqian, L. Xia, Y. Lei, F. Yu, Z. Huabei, Radiosynthesis and in-vivo evaluation of [125I]IBT: a single-photon emission computed tomography radiotracer for alpha7-nicotinic acetylcholine receptor imaging, *Nucl. Med. Commun.* 38 (2017) 683-693.
- [32] H.W. H.Wang, S.X. Wang, S.Y.Liang, J.P.Liu, H.B.Zhang, A novel fluorenone derivative labeled with [18F] as $\alpha 7$ -Nicotinic Acetylcholine Receptor PET/CT Imaging Agents, in: the 13th Radiopharmaceutical and labeled Compound Academic Exchanges meeting Beijing, China, 2016, pp. 30.
- [33] A.M. Brown, Drugs, hERG and sudden death, *Cell Calcium* 35 (2004) 543-547.
- [34] P.W. Miller, N.J. Long, R. Vilar, A.D. Gee, Synthesis of 11C, 18F, 15O, and 13N radiolabels for positron emission tomography, *Angew. Chem. Int. Ed. Engl.* 47 (2008) 8998-9033.
- [35] M. Laruelle, M. Slifstein, Y. Huang, Relationships between radiotracer properties and image quality in molecular imaging of the brain with positron emission tomography, *Mol. Imaging Biol.* 5 (2003) 363-375.
- [36] S. Patel, R. Gibson, In vivo site-directed radiotracers: a mini-review, *Nucl. Med. Biol.* 35 (2008) 805-815.
- [37] T.K. M, S.K. S, S.K. J, H.S. K, Y.H. H, K.W. Spencer, G.J. R, H. Tayyaba, P.B. W, In vivo quantification of tumor receptor binding potential with dual-reporter molecular imaging, *Mol. Imaging Biol.* 14 (2011) 584-592.
- [38] C. Gotti, F. Clementi, A. Fornari, A. Gaimarri, S. Guiducci, I. Manfredi, M. Moretti, P. Pedrazzi, L. Pucci, M. Zoli, Structural and functional diversity of native brain neuronal nicotinic receptors, *Biochem Pharmacol* 78 (2009) 703-711.
- [39] A. Karlin, M.H. Akabas, Toward a structural basis for the function of nicotinic acetylcholine receptors and their cousins, *Neuron* 15 (1999) 1231-1244.
- [40] X. Zhang, J.B. Han, P.F. Li, X. Ji, Z. Zhang, Improved, Highly Efficient, and Green Synthesis of Bromofluorenes and Nitrofluorenes in Water, *Synth. Commun.* 39 (2009) 3804-3815.
- [41] M.R.S. Schrimpf, Kevin B.; Ji, Jianguo; Li, Tao; Frost, Jennifer M.; Briggs, Clark A.; Bunnelle, William H., Preparation of amino-substituted tricyclic derivatives as modulators of $\alpha 7$ nicotinic receptors and methods of use, in, USA, 2005.
- [42] S. Gemma, C. Camodeca, M. Brindisi, S. Brogi, G. Kukreja, S. Kunjir, E. Gabbellieri, L. Lucantoni, A. Habluetzel, D. Taramelli, N. Basilico, R. Gualdani, F. Tadini-Buoninsegni, G. Bartolommei, M.R. Moncelli, R.E. Martin, R.L. Summers, S. Lamponi, L. Savini, I. Fiorini, M. Valoti, E. Novellino, G. Campiani, S. Butini, Mimicking the intramolecular hydrogen bond: synthesis, biological evaluation, and molecular modeling of benzoxazines and quinazolines as potential antimalarial agents, *J. Med. Chem.* 55 (2012) 10387-10404.
- [43] H.E. Bronstein, N. Choi, L.T. Scott, Practical synthesis of an open geodesic polyarene with a fullerene-type 6 : 6-double bond at the center:

- [44] O.H. Lowry, N.J. Rosebrough, A.L. Farr, R.J. Randall, Protein Measurement with the Folin Phenol Reagent, *J. Biol. Chem.* 193 (1951) 265-275.

ACCEPTED MANUSCRIPT

- 1 A class of 1,4-diazobicyclo[3.2.2]nonane derivatives was synthesized and evaluated as $\alpha 7$ -nAChR ligands.
- 2 Five ligands displayed high binding affinity ($K_i = 0.001$ -25 nM) for $\alpha 7$ -nAChRs.
- 3 [^{18}F]**15** displayed high binding affinity, selectivity for $\alpha 7$ -nAChRs and good pharmacokinetics in mice.